MDPI

Article

Proprioceptive estimation of forces using underactuated fingers for Robot-Initiated pHRI

Joaquín Ballesteros[1], Francisco Pastor[2], Jesús M. Gómez-de-Gabriel[2], Juan M. Gandarias[2], Alfonso J. García-Cerezo[2], Cristina Urdiales[3]

[1] Department of Computer Languages and Science; University of Malaga. Escuela de Ingeniería Informática, Málaga, Spain; jballesteros@lcc.uma.es
[2] Systems Engineering and Automation Department, University of Malaga. Escuela de Ingenierías Industriales, Málaga, Spain; {fpastor, jesus.gomez, jmgandarias, ajgarcia }@uma.es
[3] Electronics Technology Department, University of Malaga. Escuela de Ingeniería Telecomunicación, Málaga, Spain; acurdiales@uma.es
* Correspondence: jballesteros@uma.es

Version January 21, 2024 submitted to Sensors

Abstract: In Physical Human-Robot Interaction (pHRI), forces exerted by humans need to be estimated to accommodate robot commands to human constraints, preferences, and needs. This paper presents a method for the estimation of the interaction forces between a human and a robot using a gripper with proprioceptive sensing. Specifically, we measure forces exerted by a human limb grabbed by an underactuated gripper in a frontal plane using uniquely the gripper's own sensors. This is achieved via a regression method, trained with experimental data from the values of the phalanxes angles and actuator signals. The proposed method is intended for adaptive shared control in limb manipulation. Although adding force sensors provide better performance, obtained results are accurate enough for this application. This approach requires no additional hardware: it relies uniquely on the gripper motor feedback and joint angles. Also, it is computationally cheap, so processing times are low enough to allow continuous human-adapted pHRI for shared control.

Keywords: Physical Human-Robot Interaction; Force Estimation; Underactuated Grippers; Adaptation

1. Introduction

Recent trends in robotics pursue the incorporation of robotic systems among people Social robots are taking on increasing importance, mostly for care applications, i.e. helping patients [1] or elderly people [2]. Collaborative robots (i.e. cobots) are expected to cooperate in physical tasks with them (e.g. moving large objects [3]). Cooperation requires adaptation on both sides. Hence, cobots must be safe [4–6] and include force sensing capabilities to better adapt to persons' feedback and constraints.

Force sensing is particularly important in Physical Human-Robot Interaction (pHRI), where robots are expected to physically manipulate a person, e.g. rehabilitation [7], exoskeletons [8], or prosthesis [9]. In these cases, dependability and safety become a major concern [10,11], specially when it is up to the robot to intentionally touch and/or manipulate people using grippers [12]. Some of these applications include assistive robotics [13], search and rescue missions [14] and healthcare applications [15] among others. These robots need to accommodate to humans' constraints and needs via shared control. To achieve continuous, transparent adaptation, low level shared control must rely on blending the robot commands with human intention,Although accuracy in force estimation is not critical at low level, as no high precision is required and constant feedback and adaptation tend to correct minor errors, it is

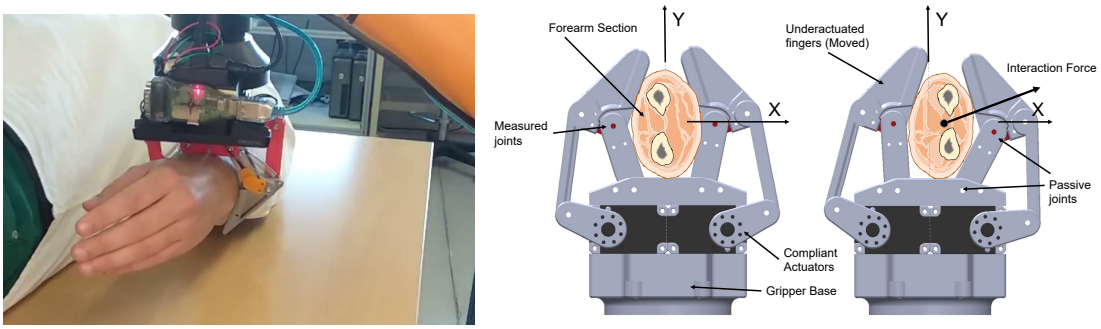

(a) (b)

Figure 1. The proposed approach estimates the forces applied by a human in a frontal plane when their forearm is grasped by a robot (a) with an underactuated gripper using only the proprioceptive information from servos and passive joint angles (b).

at least necessary to assess human force direction and magnitude, so the robot can comply with the person's input.

There are several methods for estimation of human/robot interaction forces. The most common ones are industrial force/torque sensors, current-controlled cobots and sensitive manipulators with joint torque sensors. Industrial sensors are accurate and provide Cartesian external forces but they are usually bulky, heavy and expensive. Manipulators with joint torque sensing can be implemented using elastic joints, which can be easily developed using the position error and the arm inverse Jacobian [16], but provide poor performance. Motor current-based force estimation depends on an accurate model of the arm dynamics with frictions [17]. Some other robots include rigid joints with torque sensors integrated with the controller, used to provide impedance control. Those robots are expensive and require complex control [18], and they are used mostly for research purposes. Some experimental force sensors for robot arms are based on lightweight pressure sensors such as piezoresistive sensors [19], MEMS barometric sensors [20], or optical [21], which are still under development.

Alternatively, force estimation could be performed on end effectors instead of on the robot arm Corrent choice of the end-effector is important for safe huaman manipulation. Although there are many different grippers [22], safe, reliable and autonomous grippers, sensitive enough to manipulate human limbs are still under research. Soft-grippers are receiving a growing interest in this field [23], but precise manipulation often requires an adaptive but more controllable solution. Gripper based proprioceptive sensing has been already used in pHRI and can provide a more controllable solution. In [24], variations on the forearm perimeter have been used to estimate hand postures. [25] proposes to estimate forces using uniquely proprioceptive sensors in an arm to estimate the position of a surgical instrument carried by an underactuated arm (continuous flexible or made of rigid serial links) based on the actual positions of the intermediate stages, and also the interaction forces.

The authors have already published works in the field of force sensing in pHRI [26] and intelligent tactile perception in robotics [27]. Specifically, in [28] they proposed to use additional joint angle sensors to obtain shape estimation on grasped objects for limb manipulation planning. In this work we propose to extend the capacities of the gripper in [28] to also assess forces exerted by the human forearm with no further modifications, i.e. additional sensors. Rather than building an analytic model, given the complexity of these problems, many of these methods rely on machine learning techniques. For example, in [29], interaction forces between a human and a cobot were measured using an external industrial 6-axis force sensor. In [30], the interaction force is predicted by using flexible joints with integrated force sensors, performing an estimation of the arm global friction, but the approach requires additional functional and fully calibrated force sensors in the gripper.

In this work, we propose a regression model to detect interaction forces in a gripper with two underactuated fingers with two-phalanx using uniquely its own proprioceptive joint sensors, namely servo and one passive joint angle. Specifically, the gripper is expected to manipulate the forearm of a

person in a frontal plane. The gripper adapts to the forearm of the human by design, flexing fingers and shifting forces to keep the grip. As the person moves to either comply with the robot motion or resist, finger angles and applied torque keep adapting, implicitly providing information on the direction and magnitude of human forces on the grip, as illustrated in Figure 1. The ultimate goal of our proposal is to obtain information on human intention and interaction force in a continuous way so that the robot may adapt to human needs and constrains in a transparent way via shared control in applications involving pHRI. The main novelty of our proposal is that it relies on information that grippers can provide without any additional hardware. Hence, we avoid any extra weight, cost and/or complexity in the system. Due to the non rigid properties of the human forearm and the use of machine learning methods, proprioceptive sensor information (servo and passive articulation positions) is related to forces. Hence, we can train a model using data from tests with volunteers where forces are measured using independent sensors. Thus, inexpensive underactuated grippers with different number of fingers can be used to assess human force based human intention for efficient, low level shared control in assistive robotics.

The paper is structured as follows. Section 2 presents the design of our gripper and its control system, also, its kinematic and dynamic analysis are presented. Section 4 presents the experimental setup of the system. Section 3 describes the tests done and the results obtained. Finally, these results are discussed in section 5, and conclusions and future work are provided in section 6.

2. The Underactuated gripper

This section presents our gripper design along with a kinematic and dynamic analysis. Besides, the experimental prototype and the sensing and control systems are described.

2.1. Design

The design proposed in this paper consists of using a gripper with two independent underactuated fingers, with two phalanxes and a single actuator each as shown in Figure 2. Actuators can be implemented using tendons or rigid linkages. The use of tendons (e.g. Yale OpenHand) as in [31] has been discarded for our application, due to the displacements of the internal contact surfaces of the fingers when pinching the human skin. Hence, our gripper relies on a transmission system based on rigid linkages, that also provides a more human-friendly contact.

A special feature of this design is the addition of a joint angular sensor that provides information of the values of the passive joints. This allows us to evaluate how the grip adapts to a human's upper-forearm. A prototype has been manufactured using FDM 3D-printers, and the CAD files have been made released openly in a public repository [1].

2.2. Forward kinematics

As the value of the joint positions in the adaptive fingers depends on the interaction forces with the environment, they provide information about the shape of the contact surfaces. The value of θ_2 (θ_{2l} and θ_{2r} for left and right fingers, respectively) are obtained by miniature potentiometers that measure the relative angle between the two phalanxes. The values of θ_a are obtained from the smart-servo controllers. Knowing both values, the five-bar mechanism, with fixed-length links, can be solved using trigonometric methods, so the angle of the first phalanx θ_1 can be computed.

Solving the trigonometric equations and using the auxiliary angles $\alpha_1 = \theta_1 + \gamma$, $\alpha_2 = \pi - \psi + \theta_2$ and $\alpha_a = \pi - \theta_a - \gamma$, the forward kinematics model is presented in equation (1).

$$\theta_1 = \operatorname{asin}\left(\frac{d}{f}\,\sin\left(\theta_a + \gamma\right)\right) + \operatorname{asin}\left(\frac{b}{g}\,\sin\left(\psi - \theta_2\right)\right) + \operatorname{acos}\left(\frac{f^2 + g^2 - c^2}{f\,g}\right) - \gamma \tag{1}$$

[1] /github.com/TaISLab/umahand

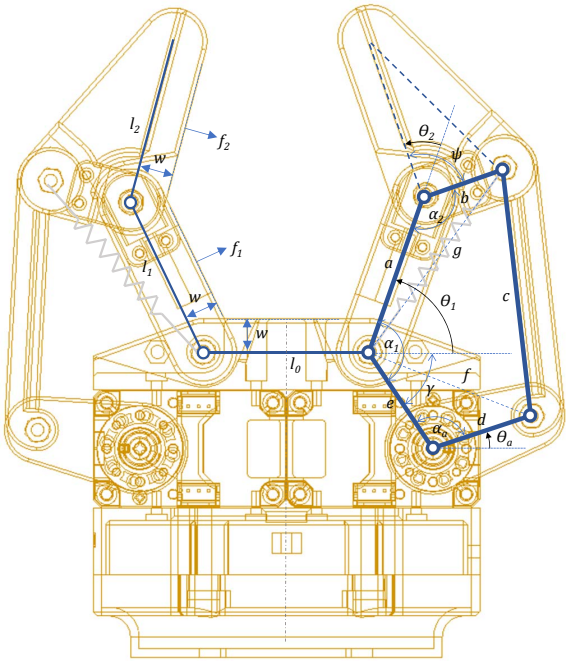

Figure 2. Kinematic design of the gripper for pHRI showing the parameters and joint angles. For clarity, every finger has been partially labeled.

where f and g are the non-adjacent vertex distances indicated in 2, computed as (2) and (3).

$$f = \sqrt{d^2 + e^2 + d\,e\,\cos(\theta_a + \gamma)} \tag{2}$$

$$g = \sqrt{a^2 + b^2 + a\,b\,\cos(\psi - \theta_2)} \tag{3}$$

2.3. Dynamic model

The general dynamic model for each of the rigid linkage-driven underactuated fingers, with multiple DOFs is given by

$$\boldsymbol{M}(\boldsymbol{\theta})\,\ddot{\boldsymbol{\theta}} + \boldsymbol{C}(\boldsymbol{\theta},\dot{\boldsymbol{\theta}})\,\dot{\boldsymbol{\theta}} + \boldsymbol{G}(\boldsymbol{\theta}) + \boldsymbol{F}(\dot{\boldsymbol{\theta}}) = \boldsymbol{T}^T(\boldsymbol{\theta})\,\tau_a + \boldsymbol{J}_1^T(\boldsymbol{\theta})\,\boldsymbol{F}_{ext_1} + \boldsymbol{J}_2^T(\boldsymbol{\theta})\,\boldsymbol{F}_{ext_2} \tag{4}$$

where $\boldsymbol{\theta} = [\theta_1\,\theta_2]^T$ is the 2×1 joint vector for each finger composed by the values of joint 1 and 2. $\ddot{\boldsymbol{\theta}}$, $\dot{\boldsymbol{\theta}}$ denote its acceleration and velocity vectors respectively. $\boldsymbol{M}(\boldsymbol{\theta})$ represents the 2×2 symmetric positive definite inertia matrix, $\boldsymbol{C}(\boldsymbol{\theta},\dot{\boldsymbol{\theta}})$ the Coriolis and centripetal torques matrix, and $\boldsymbol{G}(\boldsymbol{\theta})$ and $\boldsymbol{F}(\dot{\boldsymbol{\theta}})$ the 2×1 gravity and friction vectors. τ_a is the scalar actuator torque, $\boldsymbol{T}^T(\boldsymbol{\theta})$ is the 2×1 transposed transfer matrix that relates the velocities of the actuators to the joint velocities, $\boldsymbol{J}_1^T(\boldsymbol{\theta})$ and $\boldsymbol{J}_2^T(\boldsymbol{\theta})$ are the 2×2 transposed Jacobian matrices of the contact points on phanlax 1 and 2 respectively, where the corresponding Cartesian forces $\boldsymbol{F}_{ext_1}$ and $\boldsymbol{F}_{ext_2}$ are considered. As all the motion axes are parallel, forces in other directions are rejected by the planar kinematic constraints. This way, Cartesian forces are be expressed as a 2×1 vector of two coordinates along the finger plane.

The actuator torque τ_a is provided by a servomotor that has his own dynamics (5) and follows a proportional position control law with torque limitations, as in (6) which renders the finger compliant.

$$\tau_a = \tau_m - J_m\,\ddot{\theta}_a - B_m\,\dot{\theta}_a \tag{5}$$

$$|\,\tau_m\,| = min\{|\,(\theta_{closed} - \theta_a)K_p\,|\,, \tau_{max}\} \tag{6}$$

Where the actual position actuator is θ_a, and J_m and B_m are the moment of inertia and frictions of the servomotor respectively, that have to be taken into account, as its gear box has four spur gears with

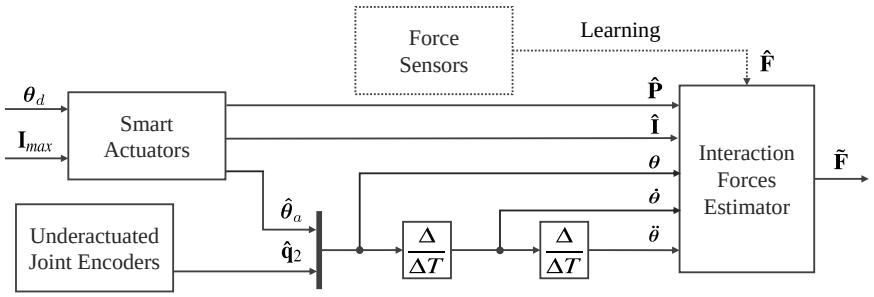

Figure 3. Representative schematic of the intelligent perception system. The regression model uses the measurements from the proprioceptive sensors of the smart actuators and the underactuated joints to estimate external forces. The dotted line represents the supervised learning process, which uses ground truth forces measured with force sensors for training.

a 350 : 1 ratio. The motor torque τ_m is computed at the embedded controller based on the following fixed parameters: reference value for the closing position θ_{closed}, proportional gain K_p, that defines the compliance, and maximum torque τ_{max} that limits the grasping force.

3. Force Estimation Method

To overcome the difficulty of obtaining an analytic model, we propose to use regression methods. The proposed method adapts better to imperfections, sensor and mechanical errors and can be extensible to other similar grippers via training. An schematic of the method is presented in Figure 3, where the symbol $(\hat{})$ represents measurements, and $\tilde{\mathbf{F}}$ are the estimated external forces.

The inputs of the smart actuators' current-based controllers are the desired position ($\boldsymbol{\theta}_d$) and maximum current ($\mathbf{I}_{max}$). Current positions ($\boldsymbol{\theta}$), velocities ($\dot{\boldsymbol{\theta}}$) and accelerations ($\ddot{\boldsymbol{\theta}}$) of the joints are considered inputs of the estimator, along with the current ($\hat{\mathbf{I}}$) and the PWM of the control signal ($\hat{\mathbf{P}}$). The position is measured from the encoders of the smart actuators ($\hat{\boldsymbol{\theta}}_a$) and the sensors integrated in the passive joints $\hat{\boldsymbol{\theta}}_2$. Velocities and accelerations are computed from the position with discrete derivatives according to the sample time (ΔT). $\hat{\mathbf{P}}$ and $\hat{\mathbf{I}}$ variables present low correlation in our actuators (Pearson coefficient equal to 0.4379) due to dynamic behavior of the DC motors. Hence, they are kept as input parameters in our model. All the signals are defined for the two-finger gripper as defined in equations (7), where sub-index r and l refer to right and left actuator, respectively.

$$\hat{\mathbf{P}} = \begin{bmatrix} \hat{p}_r \\ \hat{p}_l \end{bmatrix};\ \hat{\mathbf{I}} = \begin{bmatrix} \hat{i}_r \\ \hat{i}_l \end{bmatrix};\ \boldsymbol{\theta} = \begin{bmatrix} \theta_{ar} \\ \theta_{2r} \\ \theta_{al} \\ \theta_{2l} \end{bmatrix};\ \dot{\boldsymbol{\theta}} = \frac{\Delta \boldsymbol{\theta}}{\Delta T};\ \ddot{\boldsymbol{\theta}} = \frac{\Delta \dot{\boldsymbol{\theta}}}{\Delta T};\ \hat{\mathbf{F}} = \begin{bmatrix} \hat{f}_x \\ \hat{f}_y \end{bmatrix};\ \tilde{\mathbf{F}} = \begin{bmatrix} \tilde{f}_x \\ \tilde{f}_y \end{bmatrix} \tag{7}$$

Thus, the goal is to find a non-linear function ($\mathscr{L}$). According to equation (8), this function estimates external forces from input parameters. We propose two regression methods to obtain $\mathscr{L}$: i) Support Vector Regression (SVR) [32]; and ii) Random Forest Regression (RFR) [33].

$$\tilde{\mathbf{F}} = \mathscr{L}\left(\hat{\mathbf{P}}, \hat{\mathbf{I}}, \boldsymbol{\theta}, \dot{\boldsymbol{\theta}}, \ddot{\boldsymbol{\theta}}\right) \tag{8}$$

SVR relies on fitting the error rate within a certain threshold rather than minimising it (Principle of Maximal Margin). The main advantages of SVR is that it is a non-parametric technique, i.e. it does not depend on distributions of the underlying dependent and independent variables. Additionally, it permits for construction of a non-linear model without changing the explanatory variables, helping in better interpretation of the resultant model. RFR is a type of additive model that makes predictions by combining decisions from a sequence of base models (ensemble learning), where each based classifier is a decision tree. Unlike linear models, RF are able to capture non-linear interaction between the

Table 1. Values of the parameters of the kinematic model of the underactuated gripper described in Figure 2.

Parameter	Value	Parameter	Value
a	40 mm	e	27.8 mm
b	20 mm	ψ	90°
c	60 mm	γ	56°
d	25 mm	w	10 mm

features and the target. Both methods are appropriate to work with non-linearity and outliers, so they are good candidates to solve our problem.

4. Experimental setup

By adding proprioceptive angular sensors, the angles θ_{2l} and θ_{2r} can be measured (we use $_l$ and $_r$ subscripts for left and right fingers). Thus, given the position information provided by the servos (θ_{al} and θ_{ar}), the position of the remaining phalanxes (θ_{1l} and θ_{1r}) can be computed. As a result, the position of the gripped objects can be estimated using the θ_{2r} and the shape of the grasped object can be inferred with the positions of the two fingers θ_l and θ_r.

Two potentiometers (*muRata* SV01 10$k\Omega$ linear) have been used for the measurement of the distal joints. They have been added to the gripper as a DAQ with a 50Hz sample rate. The actuators are *Dynamixel XL450-W250* servos featuring a 12-bits digital magnetic encoder (0.088° resolution), and an advanced position based-controller with torque limits to provide a sort con force control. This capability is essential to control the grasping force. Their internal position PID loops have been set to Proportional-only control to get compliance to the user interaction forces. The servos provide real-time feedback of the positions (θ_a), the electrical current (I), and the PWM output (P) of the controller.

A microcontroller board (Arduino Mega 2560) has been used as gripper interface and DAQ, that periodically samples the analog values with 10-bits ADC (0.26° resolution), from the potentiometers, and queries the status of the servos at a rate of 10Hz. Using a serial port over USB communicates with the main computer to provide with the above information and receives simple Open/Close commands.

The actual values of the parameters for the kinematics shown in Figure 2 can be found in Table 1. It has been designed to grasp an upper-forearm with a perimeter between 16.2 and 19.3 cm and a median of 17.7 cm, according to the anthropometrics from [34].

The joints ranges present different mechanical limits. In particular $0 \geq \theta_2 \geq \pi/2$. The position of the phalanxes depends on the balance between external forces F_1, F_2, the actuator torque θ_a and the extension springs (164 N/m) used to make the finger stable when no external forces are applied.

In order to use machine learning techniques to estimate forces using the gripper, we need to capture all the problem instance parameters simultaneously. Also, we need a test environment that ensures repeatability. Hence, we have designed the structure in Figure 4 to obtain a ground truth for our regression methods. It can be observed that the gripper is physically attached to six load cells used to estimate Cartesian forces (Figure 4.a). Thus, when the gripper is closed around a moving forearm (Figure 4.b), we can record its force and all gripper parameters at the same rate of 20 Hz.

Force sensors in our structure (see Figure 5a) have been calibrated using a dummy forearm-section and a force-meter to obtain ground-truth values. Different forces at different angles have been applied (Figure 5b), and recorded together its corresponding load-cells readings. Then, a matrix that relates the six readings from the load cells has been adjusted using a least squares method. The inverse of this matrix will then be used to provide output forces in kgf units from load-cell readings.

After the calibration of the force sensor, a proportional control loop was programmed to maintain the person's forearm as close as possible to the center of the gripper. We purposefully kept a low gain in our control loop in order to be more sensitive to external perturbations.

Figure 6 shows forces measured in the X and Y axes by the load cells in the structure, the corresponding joint and servo positions and the current and PWM provided by the servo controller

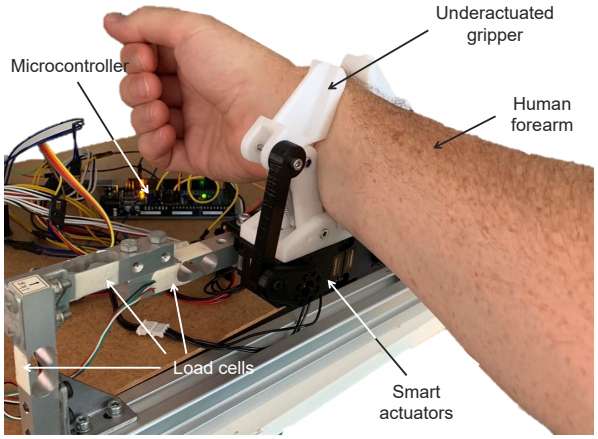

Figure 4. Illustration of the data collection process with the experimental force sensing system (left side visible only) to record ground-truth data and gripper readings to train the regression methods. Note that only three load cells (left finger) are visible in this picture as the other three (right finger) are hidden by the human forearm.

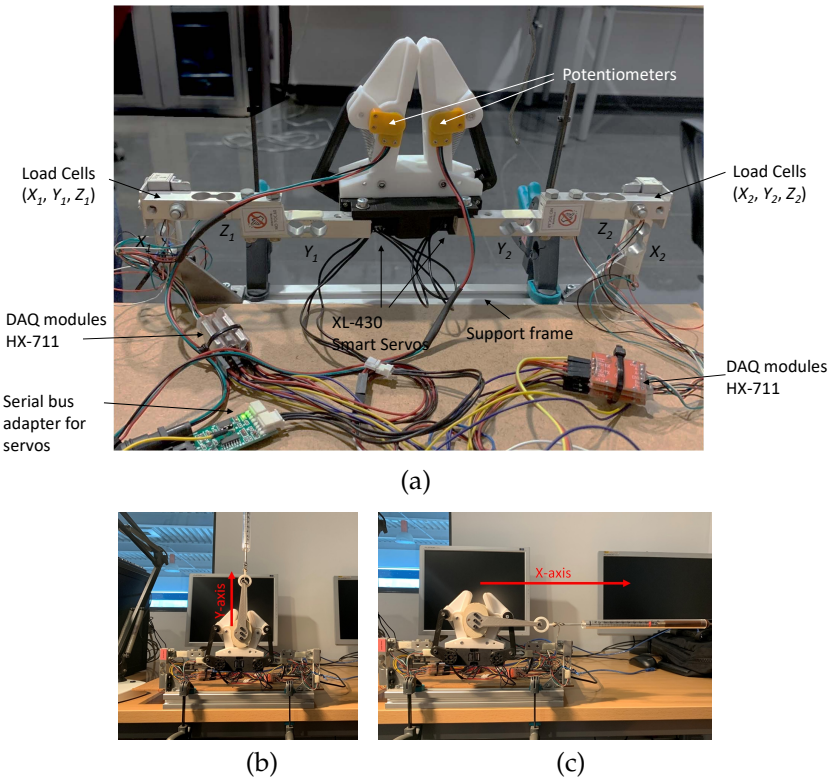

Figure 5. Experimental setup (a) and calibration process for Y-axis (b) and X-axis (c) forces. A dummy forearm-section is used to calibrate the force sensor used to get ground-truth values for the force estimation methods.

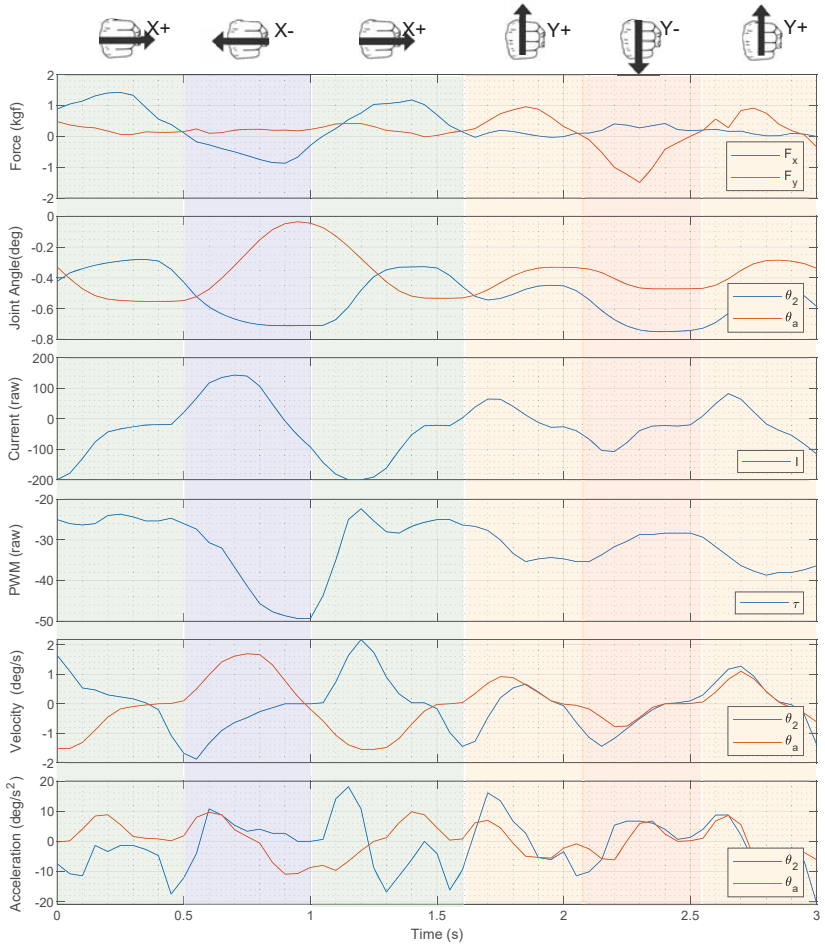

Figure 6. Excerpt from the data collected during experiments: Exerted forces (F_x, F_y) and the input parameters position (θ_2, θ_a), current (I), PWM (P), velocity ($\dot{\theta}_2$, $\dot{\theta}_a$), and acceleration ($\ddot{\theta}_2$, $\ddot{\theta}_a$), for left finger. Right finger data are analogous.

for left gripper side. Signals may be positive or negative depending on the motor direction. In this example, the person first moves his forearm 3 times right and 3 times left (X axis) and then 2 times up and 2 times down (Y axis) in a sequence. Forces during the sequence can be clearly observed as peaks in the X axes in Figure 6. It can also be observed how θ_a and θ_2 evolve with the forces. Similarly, current and PWM also present changes depending on forces. It can be observed that, in general, forces in the x-axis (e.g. seconds 1 to 3.5) are more correlated with the gripper parameter than forces in the y-axis (e.g. seconds 3.5 to 5). This was expected because the gripper is aligned in the Y axis in our tests, so the gripper fingers tend to slip when forearms move in vertical.

As commented in section 2.3, dynamic parameters are required for force estimation. We can obtain angular velocities and acceleration extracting the first and second derivatives of on θ_a, θ_2. To reduce noise in these new features, we use a moving average filter (size 3). Figure 6 shows these first and second derivatives, that present similar trends with exerted forces.

It can be observed that obtained derivatives are centred in zero, whereas θ_a, θ_2 are not. This happens because these angles depend on the gripped forearm shape. In order to avoid this shape dependence, we propose to use the initial forearm angles θ_a, θ_2, obtained when the gripped initially closes, as an offset.

5. Experimental Protocol and Results

In order to test our system, five volunteers were asked to get their forearms gripped and pull in a frontal plane (X and Y movements) to obtain a training dataset. Each volunteer performs 2-minutes

circular motion (see figure 8.b) and 2-minutes cross motion (see figure 8.a). Forces and gripper parameters were captured in a continuous way with a common time reference at 20Hz. More than 20000 samples were recorded in total.

5.1. Data modelling

Our problem requires multi-variable analysis as we need to estimate forces on the x and y axis. The first decision before modelling was consequently whether to work with forces independently or together. We have decided to model them independently; otherwise, any motion patterns in training sets presenting casual relationships in X and Y, e.g. users doing circular motion or favoring one side against the other, would be acquired in the model.

As commented, we have tested RFR and SVR to create our model. Both techniques are appropriate to deal with non-linearity (e.g. Figure 6). RFR is particularly fit to cope with problems where parameters have different importance depending on the situation. For example, when forces in the x-axis are low, the current parameter (I) does not provide much information, whereas θ_2 is still correlated with the force (Figure 6). However, SVR deals better than RFR with sparse data, which is present in boundaries -i.e. large forces- in our dataset.

Matlab[2] has been used to create RFR and SVR models. RFR has been created using the *TreeBagger* function. The best hyperparameter set for our data was: NumTrees = 40, MinLeafSize=5. SVR was created with the $fitrsvm$ function. Kernel radial with standard parameters outperforms linear and polynomial kernel for our data. Automatic parameter optimization has been used ($OptimizeHyperparameters$) to select the best values for *BoxConstraint*, *KernelScale* and *Epsilon* parameters.

5.2. Performance evaluation and discussion

In this section, we analyze force estimation results in the frontal plane (X and Y), both for RFR and SVR. To do so, we acquired information from 5 volunteers using the described system. Each volunteer performed two tests: i) exerting forces in a cross pattern (only X or Y direction at a given time), and ii) exerting forces in a circular pattern (forces both in X and Y at all times), as shown in Figure 8. Volunteers were trained to use constrained forces, although no mechanism was applied to keep them in a constrained interval Ten tests were recorded per volunteer in a total testing time of 2 minutes after training. Afterwards, a k-fold cross-validation technique per volunteer ($k = 5$) was used to evaluate the accuracy of the models. Finally, the Mean Absolute Error (MAE) was calculated for all tests of each regression model in X and Y.

Figure 7 shows the resulting Force X and Force Y estimates versus the measured force values for all tests using both methods (SVR and RFR) in terms of MAE. RFR outperforms SVR slightly for our dataset. It can be observed in the middle range both models behave similarly but in all cases that RFR provides a better fit for low and high force values. This confirms the importance of input parameters depend on the force ranges. To understand this dependence, we can observe the importance of those input parameters using the *OOBPermutedPredictionDeltaError* variable from the *TreeBagger* RFR function in Matlab (Table 2). It can be observed that current I and the servo speed $\dot{\theta}_a$ are the most relevant parameters to estimate forces in the X axis. However, in order to estimate forces in the Y-Axis the second passive joint angle θ_2 and its variation become more relevant. This is most likely due to slippage in fingers when users pull their forearm up and/or down, meaning that variations in the grip become more important than forces in the servoes in these cases.

Figure 8 shows estimates versus real force values for a single test over time. It can be observed that the force module tends to be underestimated. This effect is higher in the Y-axis compared to the X-axis (see Figure 8.b), due to slippage in the grip. It can be observed that the motion pattern is

[2] Version used: R2019a by The MathWorks, Inc.

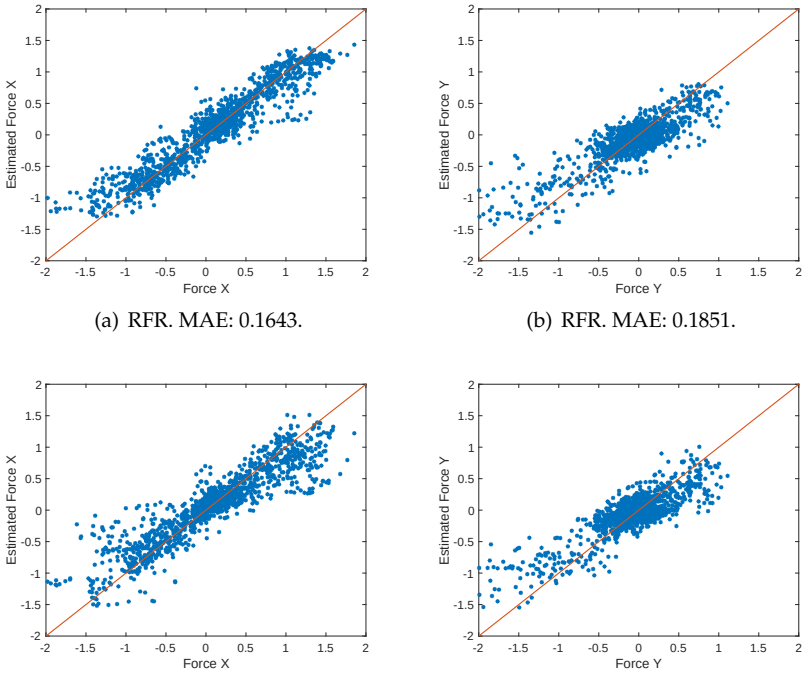

(a) RFR. MAE: 0.1643. (b) RFR. MAE: 0.1851.

(c) SVR. MAE: 0.2009. (d) SVR. MAE: 0.1905.

Figure 7. X (left) and Y (right) real cartesian forces versus estimated forces using RFR (top) and SVR (bottom) methods.

Table 2. Parameter Importance in RFR. Best parameters are outlined.

	θ_2	θ_a	I	P	$\dot{\theta}_2$	$\dot{\theta}_a$	$\ddot{\theta}_2$	$\ddot{\theta}_a$
Force X	1.0921	0.9185	**1.3562**	0.9050	0.8265	**1.3502**	0.7936	0.8949
Force Y	**1.6341**	0.7029	0.7296	0.9385	**1.5958**	0.8571	0.7358	0.7156

correctly estimated. Hence, user's intention can be estimated from these forces estimation to be used in a shared control approach, i.e. to adapt emergent motion patterns to the user's preferred direction. Typically, users' intention in shared control in pHRI have been obtained in different ways. In [35] intent is defined in a binary way (e.g., motion or not, left or right, up or down, etc.). Also, it is defined within a set of discrete intents (e.g. predefined poses) or using continuous variables (e.g steering angles). Our approach provides Cartesian X and Y forces. These forces can be transformed into polar coordinates - error module (ρ_ϵ) and angle (θ_ϵ) to calculate the classification accuracy and estimation error in all three typical user intent estimations: binary intent (left or right, i.e 180 degrees clustering), discrete intents (left, right, up and down, i.e 90 degrees clustering) and continuous intent (module and angle). Table 3 shows the results. It can be observed that the classification accuracy remains high in binary and discrete cases (above 90%), with values similar to the ones presented in [36]. On the other hand, continuous values provide a granularity below 20 degrees on average in direction, so applications that need to know the user's intention to collaborate with them in tasks with some degree of freedom -e.g. repositioning a limb vs (precise) assistive surgery- can rely on the proposed approach.

Table 3. User intent estimation depending on the desired shared-control output

Intent	**Classification accuracy/Estimation Error**			
Binary	99,08% (Right)		98.78%(Left)	
Discrete	96.34%(Right)	97.69%(Up)	94.03%(Left)	95.87%(Down)
Continuous	19.2 degrees (θ_ϵ)		0.22 kgf(ρ_ϵ)	

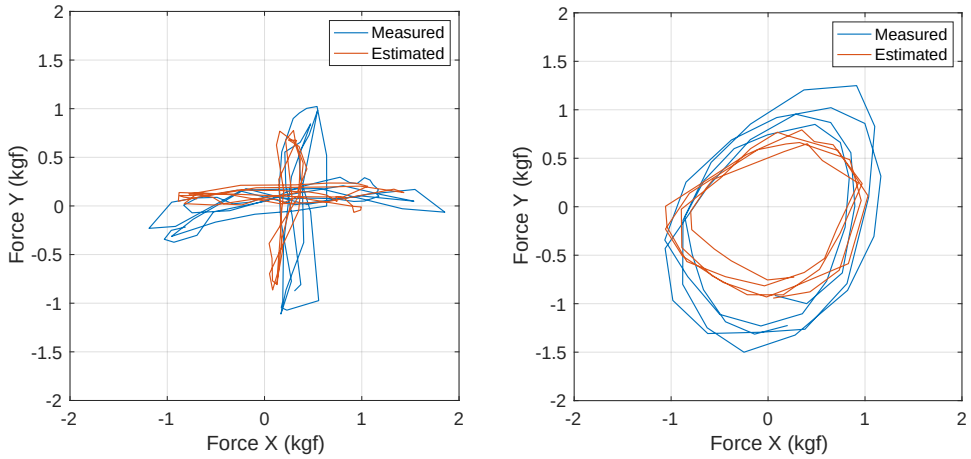

Figure 8. Estimated vs measured forces for two types of interaction experiments. a) Vertical and horizontal forces durin 4 s. b) circular forces trying to describe a circle for 2.8 s.

6. Conclusions

In this work, we have presented a method to estimate interaction forces with an underactuated gripper grasping a human forearm. These forces are related to human intention and, hence, critical for pHRI. The intention is typically used in shared control approaches to ensure that human constraints, goals, and comfort are taken into account while their forearms are being manipulated.

We use only the gripper proprioceptive sensors to estimate the forces. Specifically, we work with a gripper with two underactuated fingers to achieve an adaptive, robust, and precise grasping of human limbs operating in a closed control loop. Its proprioceptive sensors provide information about the servo and passive joint positions -using uniquely two inexpensive potentiometers-, plus the motor PWM and current. The analytical model of the gripper may already produce limited information about human forces in the gripper, but the model is only valid for certain conditions and it does not account for limb slippage nor for artifacts. Instead, we propose to use Machine Learning to estimate human forces.

We have designed a platform to capture the required learning dataset that includes a fixated gripper and a force-measurement structure to get training data. When volunteers are moving their gripped forearms, we gather all the gripper parameter values as well as the load cells readings. We tested SVR and RFR to predict forces using the acquired dataset. RFR provides slightly better results because it adapts better to the nature of our data: depending on the force range, some input parameters provide more information than others. Specifically, we observed that force in X is better estimated using I and $\dot{\theta}_a$ and force in Y is better estimated using θ_2 and $\dot{\theta}_2$. After training, the method is computationally cheap and resulting trees can be run in parallel.

The proposed method does not require any additional sensor except the gripper proprioceptive ones. Additionally, proposed proprioceptive sensors are cheap, robust, and do not require calibration for each different gripped object. The gripper has two fingers in the same plane, so only two-dimensional forces (in a frontal plane) are considered because the forces in other directions are rejected by the kinematic constraints of the fingers.

Results prove that the proposed methodology provides satisfactory results in all our tests with different people and changing forces. Future work will focus on developing a gripper with a higher number of non-parallel fingers to consider forces in the full Cartesian space. Also, we will work on implementing shared control based on estimated forces to prove that task efficiency and human comfort improve using the proposed method to estimate user's intentio.

Author Contributions: For research articles with several authors, a short paragraph specifying their individual contributions must be provided. The following statements should be used "conceptualization, J.B., F.P., J.G.G. and C.U.; methodology, J.B. and F.P.; software, J.B.; validation, J.B., J.M.G. and C.U.; formal analysis, J.B., J.M.G and C.U.; data curation, J.B., F.P.; writing–original draft preparation, J.B., F.P., J.M.G., J.G.G. and C.U.; writing–review and editing, J.B., F.P., J.M.G., J.G.G. and C.U.; visualization, J.B., F.P. and J.M.G.; supervision, A.G.C., J.G.G. and C.U. ; project administration, J.G.G. and C.U.; funding acquisition, A.G.C. and C.U."

Funding: This work was supported by the the Spanish project RTI2018-093421-B-I00, RTI2018-096701-B-C21, the European Commission under grant agreement BES-2016-078237.

Conflicts of Interest: The authors declare no conflict of interest.

References

1. Krishnaswamy, K.; Moorthy, S.; Oates, T. Survey Data Analysis for Repositioning, Transferring, and Personal Care Robots. International Conference on PErvasive Technologies Related to Assistive Environments (PETRA), 2017, pp. 45–51.
2. Krishnan, R.H.; Pugazhenthi, S. Mobility assistive devices and self-transfer robotic systems for elderly, a review. *Intelligent Service Robotics* **2014**, *7*, 37–49.
3. Nikolaidis, S.; Hsu, D.; Srinivasa, S. Human-robot mutual adaptation in collaborative tasks: Models and experiments. *The International Journal of Robotics Research* **2017**, *36*, 618–634.
4. ISO/TS 15066:2016. Robots and robotic devices - Collaborative robots (retrieved on 19.09.2019). *[Online]. Available: https://www.iso.org/standard/62996.htm*.
5. Malm, T.; Viitaniemi, J.; Latokartano, J.; Lind, S.; Venho-Ahonen, O.; Schabel, J. Safety of Interactive Robotics—Learning from Accidents. *International Journal of Social Robotics* **2010**, *2*, 221–227.
6. Gandarias, J.M.; Wang, Y.; Stilli, A.; García-Cerezo, A.J.; Gómez-de Gabriel, J.M.; Wurdemann, H.A. Open-loop position control in collaborative, modular Variable-Stiffness-Link (VSL) robots. *IEEE Robotics and Automation Letters* **2020**, *5*, 1772 – 1779.
7. Stilli, A.; Cremoni, A.; Bianchi, M.; Ridolfi, A.; Gerii, F.; Vannetti, F.; Wurdemann, H.A.; Allotta, B.; Althoefer, K. AirExGlove - A novel pneumatic exoskeleton glove for adaptive hand rehabilitation in post-stroke patients. IEEE International Conference on Soft Robotics (RoboSoft), 2018, pp. 579–584.
8. Li, Z.; Huang, B.; Ye, Z.; Deng, M.; Yang, C. Physical Human–Robot Interaction of a Robotic Exoskeleton By Admittance Control. *IEEE Transactions on Industrial Electronics* **2018**, *65*, 9614–9624.
9. Geethanjali, P. Myoelectric control of prosthetic hands: State-of-the-art review. *Medical Devices: Evidence and Research* **2016**, *9*, 247–255.
10. Bowyer, S.A.; y Baena, F.R. Dissipative control for physical human–robot interaction. *IEEE Transactions on Robotics* **2015**, *31*, 1281–1293.
11. Stilli, A.; Grattarola, L.; Feldmann, H., W.H.; Althoefer, K. Variable Stiffness Link (VSL): Toward inherently safe robotic manipulators. IEEE International Conference on Robotics and Automation (ICRA), 2017, pp. 4971–4976.
12. Chow, K.; Kemp, C.C. Robotic repositioning of human limbs via model predictive control. IEEE International Symposium on Robot and Human Interactive Communication (RO-MAN). IEEE, 2016, pp. 473–480.
13. Erickson, Z.; Clever, H.M.; Turk, G.; Liu, C.K.; Kemp, C.C. Deep haptic model predictive control for robot-assisted dressing. IEEE International Conference on Robotics and Automation (ICRA), 2018, pp. 1–8.
14. Gómez-de Gabriel, J.M.; Gandarias, J.M.; Pérez-Maldonado, F.J.; García-Nunez, F.J.; Fernandez-Garcia, E.J.; Garcia-Cerezo, A.J. Methods for Autonomous Wristband Placement with a Search-and-Rescue Aerial Manipulator. IEEE/RSJ International Conference on Intelligent Robots and Systems (IROS), 2018, pp. 7838–7844.
15. Huang, Y.; Li, J.; Huang, Q.; Souères, P. Anthropomorphic robotic arm with integrated elastic joints for TCM remedial massage. *Robotica* **2015**, *33*, 348–365.
16. Kruse, D.; Radke, R.J.; Wen, J.T. Collaborative human-robot manipulation of highly deformable materials. 2015 IEEE International Conference on Robotics and Automation (ICRA), 2015, pp. 3782–3787. doi:10.1109/ICRA.2015.7139725.

17. Wahrburg, A.; Bös, J.; Listmann, K.D.; Dai, F.; Matthias, B.; Ding, H. Motor-Current-Based Estimation of Cartesian Contact Forces and Torques for Robotic Manipulators and Its Application to Force Control. *IEEE Transactions on Automation Science and Engineering* **2018**, *15*, 879–886. doi:10.1109/TASE.2017.2691136.
18. Chawda, V.; Niemeyer, G. Toward torque control of a KUKA LBR IIWA for physical human-robot interaction. 2017 IEEE/RSJ International Conference on Intelligent Robots and Systems (IROS), 2017, pp. 6387–6392. doi:10.1109/IROS.2017.8206543.
19. Radó, J.; Dücső, C.; Földesy, P.; Szebényi, G.; Nawrat, Z.; Rohr, K.; Fürjes, P. 3D force sensors for laparoscopic surgery tool. *Microsystem Technologies* **2018**, *24*, 519–525.
20. Guggenheim, J.W.; Jentoft, L.P.; Tenzer, Y.; Howe, R.D. Robust and Inexpensive Six-Axis Force–Torque Sensors Using MEMS Barometers. *IEEE/ASME Transactions on Mechatronics* **2017**, *22*, 838–844. doi:10.1109/TMECH.2017.2654446.
21. Chen, S.; Wang, J.; Kazanzides, P. Integration of a Low-Cost Three-Axis Sensor for Robot Force Control. 2018 Second IEEE International Conference on Robotic Computing (IRC), 2018, pp. 246–249. doi:10.1109/IRC.2018.00052.
22. Yang, C.; Zeng, C.; Liang, P.; Li, Z.; Li, R.; Su, C.Y. Interface design of a physical human-robot interaction system for human impedance adaptive skill transfer. *IEEE Transactions on Automation Science and Engineering* **2018**, *15*, 329–340.
23. Shintake, J.; Cacucciolo, V.; Floreano, D.; Shea, H. Soft Robotic Grippers. *Advanced Materials* **2018**, *30*.
24. Choi, H.; Lee, S. Improving the performance of hand posture classification by perimeter sensor with sEMG. 2013 IEEE International Conference on Mechatronics and Automation, 2013, pp. 819–824. doi:10.1109/ICMA.2013.6618021.
25. Larkin, D.Q.; Duindam, V. Arm with a combined force and shape sensor, 2018. US Patent App. 10/105,188.
26. Gómez-de Gabriel, J.; Harwin, W. Evaluation of sensor configurations for robotic surgical instruments. *Sensors* **2015**, *15*, 27341–27358.
27. Gandarias, J.M.; Gómez-de Gabriel, J.M.; García-Cerezo, A.J. Enhancing Perception with Tactile Object Recognition in Adaptive Grippers for Human–Robot Interaction. *Sensors* **2018**, *18*, 692.
28. Gandarias, J.M.; Pastor, F.; Muñoz-Ramírez, A.J.; García-Cerezo, A.J.; Gómez-de Gabriel, J.M. Underactuated Gripper with Forearm Roll Estimation for Human Limbs Manipulation in Rescue Robotics. IEEE/RSJ International Conference on Intelligent Robots and Systems (IROS), 2019, pp. 5937–5942.
29. Peternel, L.; Fang, C.; Tsagarakis, N.; Ajoudani, A. Online Human Muscle Force Estimation for Fatigue Management in Human-Robot Co-Manipulation. IEEE/RSJ International Conference on Intelligent Robots and Systems (IROS), 2018, pp. 1340–1346.
30. Liu, X.; Zhao, F.; Ge, S.S.; Wu, Y.; Mei, X. End-Effector Force Estimation for Flexible-Joint Robots With Global Friction Approximation Using Neural Networks. *IEEE Transactions on Industrial Informatics* **2019**, *15*, 1730–1741. doi:10.1109/TII.2018.2876724.
31. Ma, R.R.; Odhner, L.U.; Dollar, A.M. A modular, open-source 3D printed underactuated hand. IEEE International Conference on Robotics and Automation (ICRA), 2013, pp. 2737–2743.
32. Jović, S.; Danesh, A.S.; Younesi, E.; Aničić, O.; Petković, D.; Shamshirband, S. Forecasting of underactuated robotic finger contact forces by support vector regression methodology. *International Journal of Pattern Recognition and Artificial Intelligence* **2016**, *30*, 1659019.
33. Liaw, A.; Wiener, M.; others. Classification and regression by randomForest. *R news* **2002**, *2*, 18–22.
34. NASA. Std-3000. Man-Systems Integration Standards. 1995, Vol. 3.
35. Losey, D.P.; McDonald, C.G.; Battaglia, E.; O'Malley, M.K. A review of intent detection, arbitration, and communication aspects of shared control for physical human–robot interaction. *Applied Mechanics Reviews* **2018**, *70*.
36. Wang, X.; Yu, H.; Li, K.; Dong, Q.; Huang, X. Study on Force Interaction System of Upper Limb Rehabilitation Robot. IOP Conference Series: Materials Science and Engineering. IOP Publishing, 2019, Vol. 631, p. 032051.